Pre-print: Version April 20, 1995

orbits Close to Asteroid 4769 Castalia

D.J. Scheeres, S.J. Ostro
Jet Propulsion Laboratory
California institute of Technology
Pasadena, CA
E-Mail:djs@leelanau.jpl.nasa.gov
R.S. Hudson
Washington State University
R.A. Werner
University of Texas at Austin

Abstract

We use a radar-derived physical model of the kilometer sized, uniformly rotating asteroid 4769 Castalia (1989 PB) to investigate close orbit dynamics. We establish that a Jacobi integral exists for particles orbiting this **asteroid,** and the attendant zero **velocity** surfaces are generated and examined. We find families **of** periodic **orbits** and determine their stability. We find that all synchronous orbits and direct orbits within ~ 3 mean radii of Castalia are unstable and are subject to impact or escape from Castalia. We find that **retrograde orbits are** mostly stable and **allow** particles to orbit closely to the asteroid **surface.**

We derive a model which allows us to predict the escape conditions of a particle in orbit about Castalia and the capture conditions of a hyperbolic interloper. Orbits within 1.5 km of Castalia are subject to immediate ejection from the system. Hyperbolic orbits with a V_∞ <0.4 m/s can potentially be captured by Castalia **if** their periapsis **radius is** within ~ 2 km. For Castalia this capture region is small, but the results also apply to larger asteroids whose capture regions would be larger in general.

We determine bounds on ejecta speeds which either ensure ejecta escape or re-impact **as a** function of location on Castalia's surface. The ejecta speeds which ensure escape range from 0.35 to 0.65 m/s over the asteroid's surface. The ejecta speeds which ensure re-impact range from 0 to 0.15 m/s over the surface. Ejecta speeds between these two bounds lead to either escape, re-impact or potentially finite time stable orbits. We develop a simple criterion which can establish whether a particle could have been ejected from the asteroid in the past or if it will impact the surface in the future.

The methods of analysis we develop in this paper are applicable to **all** uniformly rotating asteroids. They provide a basis from which systematic studies of particle dynamics close to uniformly rotating **asteroids** can be launched.

1 Introduction

In the near future an increasing number of small, near Earth asteroids will have their shape and rotational dynamics estimated using ground-based range-doppler radar imaging. The intent of this paper is to provide a detailed look at the orbital dynamics associated with Asteroid 4769 Castalia (1989 PB), and to develop general analysis tools which can describe these dynamics in a meaningful way. Such an investigation will hopefully provide the basis for future investigations of uniformly rotating asteroids when these data sets become more common.

The gravity field near this kilometer-sized Earth-crosser is modeled by combining a radar- derived 3-D shape model (Hudson & Ostro 1994), an assumed uniform density of 2.1 g/cc, and a 4.07-hour rotation about the model's largest moment of inertia, The gravity field can be expressed in clod form as a polyhedron or in terms of standard gravitational harmonic coefficients.

In this paper we explore close-or])it dynamics around the kiloltlcter-sized object 4769 Castalia (1989 PB), the first Earth-crossing asteroid for which a realistic shape model exists. A detailed understanding of the dynamics of orbits close to small (kilometer sized), irregularly shaped asteroids is required for realist, ic investigation of the systematics of cratering ejecta and the evolution of those objects' regoliths. The stability of close orbits bears on questions about possible satellites of small bodies and on the practical challenge of maneuvering spacecraft near the surfaces of such targets as Earth-approaching asteroids. Several authors have touched 011 the issue of close-orl]it dynamics (Chauvineau et al., 1994, Cintala et al., 1979, Dobrovolskis & Burns, 1980, Scheeres 1994 & 1995, Weidenshilling et al., 1989, Harris, 1987, Geissler et al., 1994, Petit et al., 1994) and a few studies have examined some of the relevant physics [WHAT DOES THIS MEAN?]. However, the previous dynamics literature has used simplistic shape models in general (ellipsoids) or has not dealt with the full nature of the dynamics of particles near an irregular shape.

Section 2 describes the generation and description of the Castalia shape, rotational dynamics and density model. Then we state the general equations of motion of a particle about such an asteroid, discuss the integrals of motion of these collations, and express the dynamic equations in terms of the osculating elements.

With this base information a number of dynamical results for the shape model are derived and discussed in Section 3. First we calculate zero velocity surfaces of the asteroid and explain the relevant information which can be obtained from them. Next we compute families of periodic orbits and determine their stability obtaining general insights into particle motion in various regimes about the asteroid. Then we derive some genera] results on the dynamics of near-equatorial orbits. This analysis enables us to estimate under what conditions a passing hyperbolic particle could become captured by Castalia, and conversely under what conditions an orbiting particle could be ejected from the Castalia system. For completeness we review the dynamics of particles in retrograde orbits. It is seen that such orbits may be qualitatively described using simple formulae.

We also confront several issues associated with trajectories of cratering ejecta and regolith evolution in general. First we discuss the local slopes on the Castalia surface in the context of the gravity field and centripetal accelerations. Then we develop a criterion which can discriminate whether or not an orbiting particle could have originated from the surface of Castalia. This criterion is useful in establishing whether a co-orbital could be an ejecta of the asteroid or if could impact the asteroid surface in the future. We characterize the evolution of ejecta from the surface of Castalia. To this end, estimates of the speed above which an ejecta will definitely escape the Castalia system as well as estimates of the speed below which an ejects will definitely fall back onto the surface of Castalia are defined as a function of position 011 Castalia's surface. Finally we examine the possibility of ejecta being trapped in stable orbits and draw conclusions about the likely distribution of re-impact ejecta on the surface.

Some specific orbital results have been generated about the Castalia model and recorded in video format (DeJong, 1995). This video depicts several different particle orbits in inertial, Castalia-fixed or particle-fixed viewpoints. It is useful for visualizing. the dynamics of particles about a small asteroid such as Castalia. Included in the video are segments depicting ejects return and escape orbits, stable retrograde orbits, unstable polar periodic orbits (at varying densities) and a hypothetical landing orbit for a powered spacecraft.

2 Castalia Model and Gravity Field

Hudson and Ostro (1994) used techniques first described by Hudson (1993) to invert delay-lh]]])]cr radar images of Castalia that had been obtained at Arecibo in 1989 by Ostro *et al.* (1990). Their inversion yielded a 167-parameter, 3-D shape model that is bifurcated into two distinct, irregular, Iiiloltlcter-sized lobes separated by a crevice that has an average depth of at least 100 m and is oriented nearly perpendicular to the asteroid's dimension. This inversion assumed uniform density and principal-axis rotation to ensure plausible extrapolation of the reconstructed surface into the (polar) region not seen by the radar. In this paper we adopt the shape model of Hudson and Ostro as a global estimate of the shape of Castalia realizing that quantitative results stated for the southern regions arc not well-collstrainccl but are merely plausible estimates. The asteroid's rotation period, estimated from the radar images and also from optical light curves (Hudson, Ostro and Harris, 1995, in prep.), is 4.07 h. The model's volume is 0.671 km^3, which corresponds to a mean radius of 0.543 km. A contour plot of the radius of Castalia is shown in Figure 1.

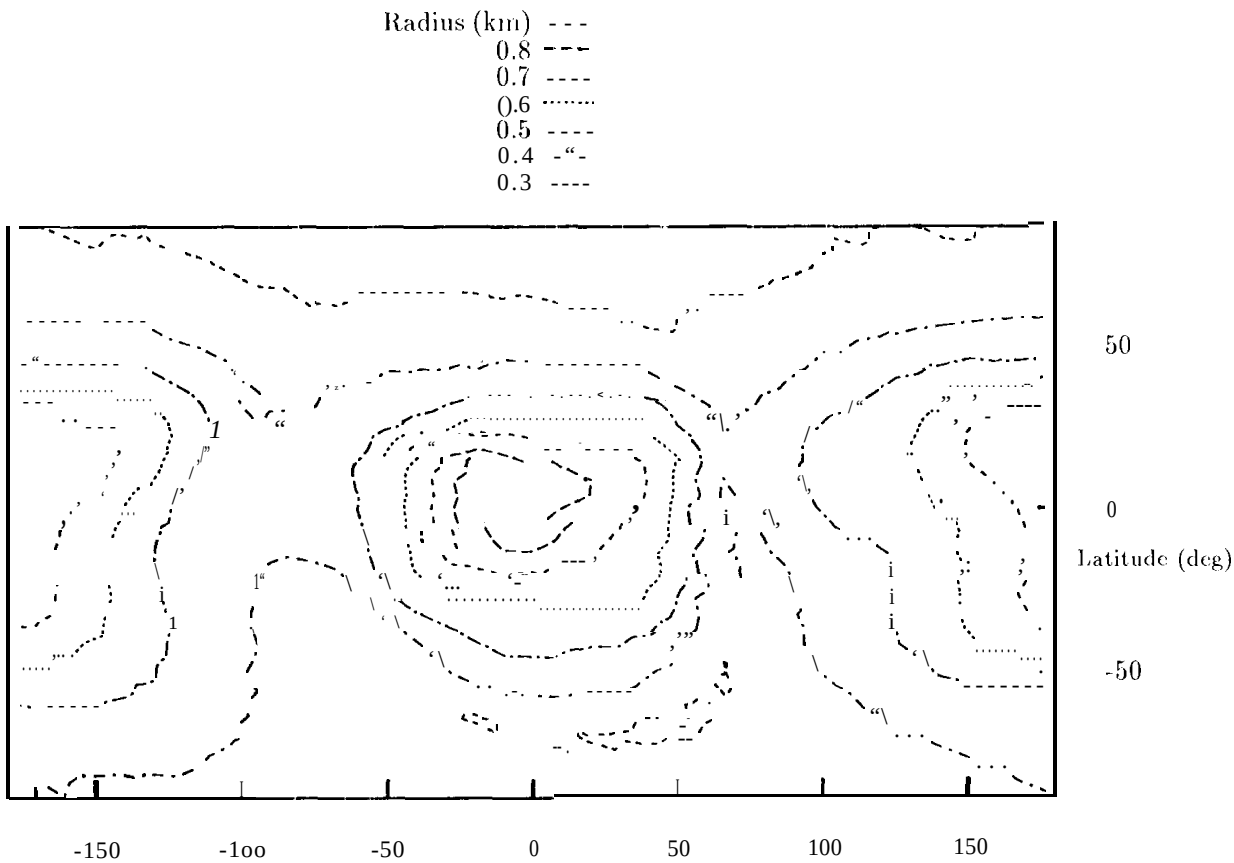

Figure 1: Radius Contours of Castalia

For describing positions about Castalia we use a body-fixed coordinate system whose origin is at the II rodel's centroid and whose axes $(x, y, 2)$ correspond to the principal axes of smallest, intermediate and its largest moment of inertia, respectively. The model's rotation pole lies along the 2-axis and its shape fits into the bounding box, centered at its center of mass,

$-0.762 < x \leq 0.851$, $-0.462 < y \leq 0.519$, $-0.444 \leq z \leq 0.382$. The ratios of the moments of inertia are:

$$I_x/I_z = 0.37207 \quad (1)$$

$$I_y/I_z = 0.93805 \quad (2)$$

An estimate of Castalia's density is derived using the following argument. First, estimates of Castalia's radar cross section and polarization ratio, when interpreted in the context of the Hudson and Ostro, 1994 modeling (see footnote 13 of that reference), suggests that the asteroid's radar albedo due to single back reflections from smooth surface elements is within 40% of 0.12. That albedo is a first approximation to the Fresnel power-reflection coefficient R, which in turn (in this situation) can be related to surface bulk density ρ through empirical formulae like

$$\rho(R) = (R + 0.13)/0.12 \quad (3)$$

This logic leads to an interval, $1.7 < \rho \leq 2.5$ g/cm^3, for the smooth component of Castalia's surface. We adopt a nominal value of 2.1, which corresponds to respective porosites of 60% and 40% for ordinary chondrites and stony irons, the candidate meteorite analogs for S class asteroids like Castalia.

That density gives a total mass

$$M = 1.4091 \times 10^{12} \text{ kg} \quad (4)$$

and a gravitational parameter

$$\mu = GM = 9.40 \times 10^{-8} \text{ km}^3/\text{s}^2 \quad (5)$$

where $G = 6.67259 \times 10^{-20}$ km^3/kg/s^2.

There are two practical approaches for generating the corresponding constant density gravitational field. The more common one determines the coefficients of a harmonic expansion of the gravity field. As is known classically (MacMillan, 1930), the gravitational field of any arbitrary body may be expressed as an infinite series expansion. The determination of these series coefficients is performed by repeatedly integrating over the entire volume of the shape, one integration for each coefficient. If constant density is assumed, these volume integrations may be reduced to integrations over the surface of the body. The most important terms of the harmonic expansion of the gravity field correspond to the C_{20} and C_{22} coefficients. For the Castalia model these are found to be:

$$C_{20} = -7.275 \times 10^{-2}/r_o^2 \quad (6)$$

$$C_{22} = 2.984 \times 10^{-2}/r_o^2 \quad (7)$$

where r_o is an arbitrary normalization radius. In the appendix is a brief description of the gravity field expansion and a table giving the gravitational coefficients up to order 4. The computations used in this paper use gravitational coefficients up to order 16. The approximation error is usually small if sufficient terms are kept. If the gravity field is evaluated close to or within the nominal radius chosen for the body then the error may become larger as the higher order gravitational terms then carry relatively more weight,. For the Castalia gravity field a normalization radius of .5431 km is used, which is the mean radius of the body.

Another approach is to use a polyhedral shape approximation and the exact closed form expression of the gravitational field of a polyhedron (Werner, 1994). This approach is especially attractive when evaluation of the gravity field must be made close to or on the surface of the asteroid. In this situation there are no singularities in the interior of the gravity field, as this formulation satisfies Poisson's equation in the interior of the body. The disadvantage of this approach is the computational time required. Every time the potential (or accelerations) are

evaluated, a summation over every face of the polyhedral shape must be performed. This is equivalent to computing one coefficient in the harmonic expansion. Th us, if the accelerations are to be computed over some time span, it is clearly more efficient to use a harmonic expansion. However this formulation is well suited to running ou a parallel computer.

3 Equations of Motion and Conserved Quantities

Given a gravitational field and the rotational state of the model, the equations of motion may be written. The most efficient expression of these equations is given in the l~ody-fixed frame of the asteroid. Given an integrated result in this frame, it is easy to transform to the inertial frame if desired. The benefit of this formulation is that no rotational transformations must be made to evaluate the gravitational accelerations and that the equations of motion are time invariant for a uniformly rotating central body.

For the general rotation of an asteroid the body fixed equations of motion for a small particle are (Greenwood, 1965, pp 50-51):

$$\ddot{\mathbf{r}} + 2\Omega \times \dot{\mathbf{r}} + \Omega \times (\Omega \times \mathbf{r}) + \dot{\Omega} \times \mathbf{r} = U_{\mathbf{r}} \tag{8}$$

where $\mathbf{r}$ is the lmdy-fixed vector from the asteroid center of mass, (--) and ($\ddot{--}$) are first and second time derivatives with respect to the body-fixed, rotating frame, Ω is the instantaneous rotation vector of the asteroid with magnitude $|\Omega| = w$, and $U_{\mathbf{r}}$ *is* the gradient of the gravitational potential $U(\mathbf{r})$ which is time-invariant in a body-fixd frame.

'1'0 analyze the dynamical equations it is of interest to find conserved quantities, or integrals. Define the function J:

$$J = \frac{1}{2}\dot{\mathbf{r}} \cdot \dot{\mathbf{r}} - \frac{1}{2}(\Omega \times \mathbf{r}) \cdot (\Omega \times \mathbf{r}) - \mathbf{U(r)} \tag{9}$$

where all the quantites arc as defined previously. Take the time derivative of this function, performing all differentiations with respect to the body-fixed frame:

$$\dot{J} = \dot{\mathbf{r}} \cdot \ddot{\mathbf{r}} - (\Omega \times \mathbf{r}) \cdot \left(\dot{\Omega} \times \mathbf{r}\right) - (\Omega \times \mathbf{r}) \cdot (\Omega \times \dot{\mathbf{r}}) - U_{\mathbf{r}}(\mathbf{r}) \cdot \dot{\mathbf{r}} \tag{10}$$

Next, take the dot product of Equation 8 with $\dot{\mathbf{r}}$ and re-arrange the results:

$$\dot{\mathbf{r}} \cdot \ddot{\mathbf{r}} - (\Omega \times \mathbf{r}) \cdot (\Omega \times \dot{\mathbf{r}}) + \dot{\mathbf{r}} \cdot \left(\dot{\Omega} \times \mathbf{r}\right) \cdot U_{\mathbf{r}}(\mathbf{r}) \cdot \dot{\mathbf{r}} = 0 \tag{11}$$

Combine Equations 10 and 11 to obtain:

$$\dot{J} = \dot{\Omega} \cdot (\mathbf{v}_I \times \mathbf{r}) \tag{12}$$

$$\text{v]} = \dot{\mathbf{r}} + \Omega \times \mathbf{r} \tag{13}$$

where $\mathbf{v}_I$ is the inertial velocity of the test particle. If the asteroid is in principal axis rotation (i.e. $\dot{\Omega} \equiv$ O) then the quantity J *is* conserved, and is in fact the Jacobi integral for the equations of motion. Thus uniform rotation of the asteroid implies that au integral of the motion exists. An equivalent statement is that the equations of motion (in the body-fixed frame) arc time invariant when $\dot{\Omega} \equiv$ o.

Since Castalia is a uniformly rotating asteroid, henceforth we assume the Jacobi function to be constant unless otherwise noted. '1'bus, given an initial particle position and velocity, the Jacobi function $J(\mathbf{r}, \dot{\mathbf{r}})$ *is* constant, for all ensuing motion of that particle. There are a variety of initial conditions which may lead to the same constant value of the Jacobi function, so it is useful to define the Jacobi constant C such that:

$$J(\mathbf{r}, \dot{\mathbf{r}}) + C = O \tag{14}$$

Recall the standard definition of the Keplerian (or two-body) energy

$$C_2 = \frac{1}{2}\mathbf{v}_I \cdot \mathbf{v}_I - \frac{\mu}{|\mathbf{r}|} \tag{15}$$

where $\mathbf{v}_I$ is the inertial velocity vector of the particle, μ is the gravitational parameter of the attracting body and $|\mathbf{r}|$ is the Euclidian norm of the particle position vector. Let us express this quantity in the body-fixed, rotating reference frame using the substitution: $\mathbf{v}_I = \dot{\mathbf{r}} + \Omega \times \mathbf{r}$. Also, assume that the gravity force potential U of the asteroid is expressed as:

$$U(\mathbf{r}) = \frac{\mu}{|\mathbf{r}|} + \sum_i U_i(\mathbf{r}) \tag{16}$$

where the U_i terms correspond to all the higher degree and order harmonics of the general gravity field. Then the Keplerian energy is:

$$C_2 = \frac{1}{2}\dot{\mathbf{r}} \cdot \dot{\mathbf{r}} - U(\mathbf{r}) + \dot{\mathbf{r}} \cdot (\Omega \times \mathbf{r}) + \frac{1}{2}(\Omega \times \mathbf{r}) \cdot (\Omega \times \mathbf{r}) + \sum_i U_i(\mathbf{r}) \tag{17}$$

Substitution of the formal Jacobian integral (Equation 14) into the above equation yields the result:

$$C_2 = \sum_i U_i(\mathbf{r}) + (\Omega \times \mathbf{r}) \cdot (\dot{\mathbf{r}} + \Omega \times \mathbf{r}) - C \tag{18}$$

where $C = -J$ is the Jacobian constant, Take the time differential of the Keplerian energy to find:

$$\dot{C}_2 = \sum_i \nabla U_i(\mathbf{r}) \cdot \dot{\mathbf{r}} + [i\text{-}l\ 2\Omega \times \dot{\mathbf{r}}](\Omega \times \mathbf{r}) \tag{19}$$

Substitute in Equations 8, noting that $\nabla(\mu/|\mathbf{r}|) = \mu\mathbf{r}/|\mathbf{r}|^3$, to find the final result:

$$\dot{C}_2 = \sum_i \nabla U_i(\mathbf{r}) \cdot \mathbf{v}_I \tag{20}$$

$$\mathbf{v}_I = \dot{\mathbf{r}} + \Omega \times \mathbf{r} \tag{21}$$

where the inertial velocity vector $\mathbf{v}_I$ may also be expressed as:

$$\mathbf{v}_I = \frac{er^2 \dot{f} \sin f}{a(1-e^2)}\hat{\mathbf{r}} + r\dot{f}\hat{\mathbf{v}}_T \tag{22}$$

with $\hat{\mathbf{v}}_T$ the unit component of the velocity normal to the radius vector. This result may also be restated in the more intuitive form:

$$\dot{C}_2 = \sum_i U_i'(\mathbf{r}) \tag{23}$$

where the U_i' term denotes the time derivative of $[J_i$ with respect to the inertial frame.

In terms of the osculating Keplerian elements, the two-body energy is:

$$C_2 = -\frac{\mu}{2a} \tag{24}$$

where a is the osculating semi-major axis of the orbit. Taking the time derivative of this and using Equation 23 results in:

$$\dot{a} = \frac{2}{n^2 a}\sum_i U_i' \tag{25}$$

where n is the mean motion of the orbit ($n = \sqrt{\mu/a^3}$). One also has from the Lagrange planetary equations the result (Kaula):

$$\dot{a} = -\frac{2}{na}\frac{\partial \sum_i U_i}{\partial M} \tag{2G}$$

where M is the mean anomaly of the orbit. From Equations 25 and 26 we find:

$$\frac{\partial \sum_i U_i}{\partial M} = \frac{1}{n}\sum_i U_i(\mathbf{r})' \tag{27}$$

which is useful as it is sometimes desired to avoid the mean anomaly in deriving explicit forms for the Lagrange equations.

Equations for the osculating periapsis and apoapsis can be derived to be [Kaula]):

$$\dot{r}_p = -\frac{(1-e)^2}{nae}\sum_i U_{i_M} + \frac{\sqrt{1-e^2}}{nae}\sum_i U_{i_\nu} \tag{28}$$

$$\dot{r}_a = \frac{(1+e)^2}{nae}\sum_i U_{i_M} - \frac{\sqrt{1-e^2}}{nae}\sum_i U_{i_\nu} \tag{29}$$

where ν is the argument of periapsis.

For the Castalia model (or any uniformly rotating asteroid) the equations of motion in scalar form reduce to:

$$\ddot{x} - 2\omega\dot{y} = \omega^2 x + U_x \tag{30}$$

$$\ddot{y} + 2\omega\dot{x} = \omega^2 y + U_y \tag{31}$$

$$\ddot{z} = U_z \tag{32}$$

The Jacobi constant C is explicitly calculated as:

$$C = V(x, y, z) - T_E \tag{33}$$

where

$$V(x, y, z) = \frac{1}{2}\omega^2(x^2 + y^2) + U(x, y, z) \tag{34}$$

is the modified potential and

$$T_E = \frac{1}{2}(\dot{x}^2 + \dot{y}^2 + \dot{z}^2) \tag{35}$$

is the kinetic energy of the particle with respect to the rotating asteroid.

4 Dynamics About Castalia

In the absence of solar perturbations, the orbital dynamics of a particle far from Castalia approach those for the classical case of motion about an oblate planet (Scheeres, 1994). Close to Castalia, however, this comparison is no longer valid and the orbits may exhibit unstable and even chaotic behavior (Chauvineau et al., 1994). There are several approaches that can illuminate the dynamics and the general structure of phase space in this situation.

4.1 Zero-Velocity Surfaces

Zero-velocity surfaces, defined using the Jacobi integral, provide concrete information regarding the possible motion of a particle. Since $T_V \geq 0$ it is possible to define an inequality

$$V(x, y, z) \geq C \tag{36}$$

that partitions the x, y, z space into regions where the particle may be found and where it may not be found, given a specific value of C. Note that $V(x, y, z) \geq 0$ over the entire space. Thus, if $C < 0$, the inequality is identically satisfied and there are no *a priori* constraints on where the particle may be found.

If $C > 0$, there will be regions of space where the inequality is violated, and hence where no particle may travel. When these forbidden regions separate space into disjoint regions a particle can never travel between these regions, no matter what its initial conditions are. The general situation is discussed more fully in (Scheeres, 1994), where the central body is assumed to be a tri-axial ellipsoid.

Zero-velocity surfaces are defined by the equation:

$$V(x, y, z) = c \tag{37}$$

This equation defines a 2-dimensional surface in the 3-dimensional x-y-z space. As the value of the Jacobi constant C is varied, the surfaces change. At critical values of C the surfaces intersect or close in upon themselves at points in the x-y-z space usually called equilibrium, or critical, points. Following in Figures 2-4 are projections of the zero-velocity surface onto the $z = 0$, $y = 0$ and $x = 0$ planes respectively. The surfaces are all evaluated close to the critical values of C. The zero-velocity curves presented here may be interpreted in much the same way as for the restricted 3-body problem (Hamilton & Burns, 1991).

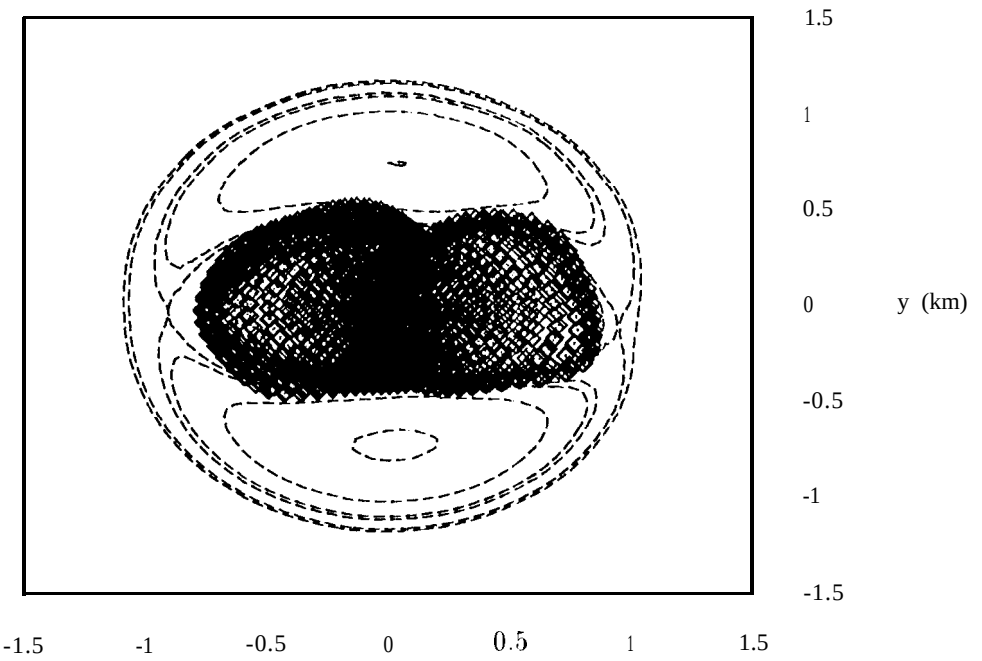

Figure 2: Zero-Velocity Curve in the x, y, 2:: 0 Plane

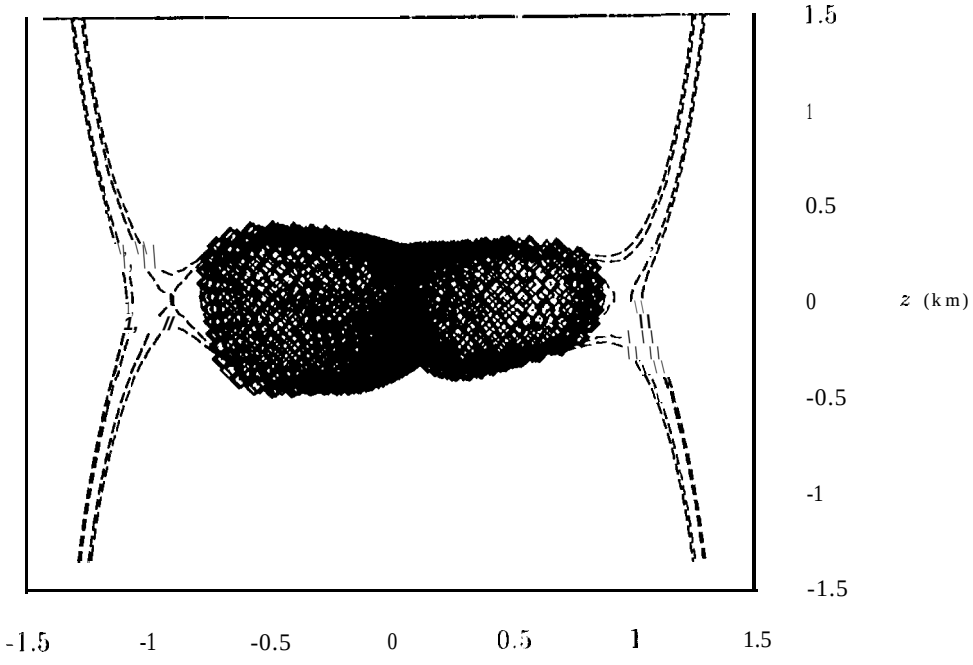

Figure 3: Zero-Velocity Curve in the $x, z, y = 0$ Plane

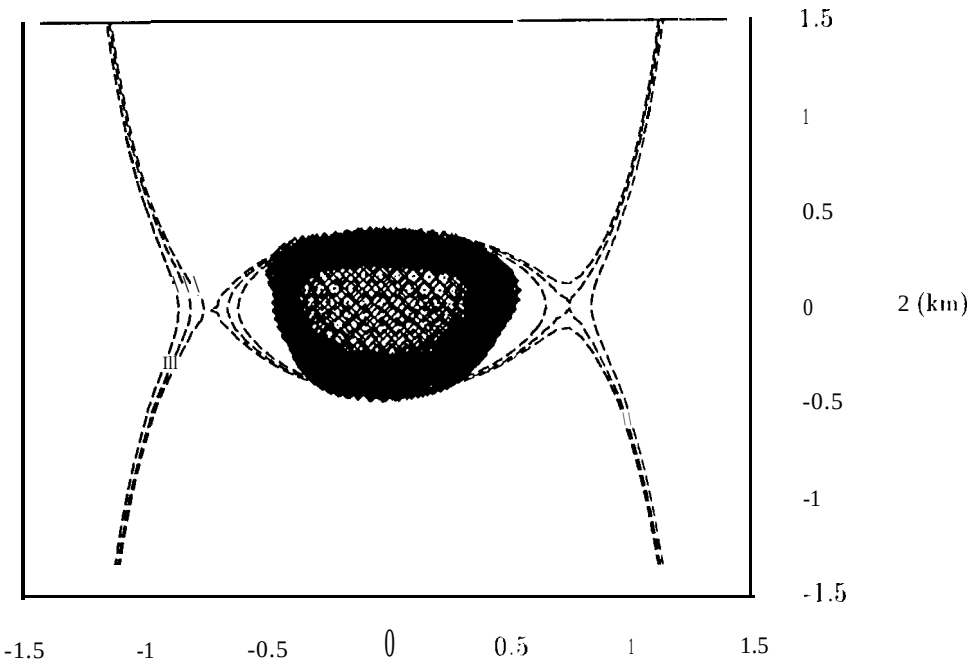

Figure 4: Zero-Velocity Curve in the y, 2, x = 0 Plane

4.2 Synchronous Orbits and Stability

Clearly seen in Figure 2 are four critical points, all of which lie near the equator and are separated by approximately 900 in longitude. At these points there is a net zero acceleration acting on the particle in the rotating frame, thus a particle placed there will ideally remain in such an orbit indefinitely. These are truly circular orbits which are exactly synchronous with Castalia's rotation rats.

A more direct manner of computing these equilibrium points is to find all the solutions of $V_{\mathbf{r}}(\mathbf{r}) = 0$. For a general gravity field there are no *a priori* number of solutions to this equation, the number of solutions depends on the shape and spin rate of the body. For Castalia there are only 4 solutions. Call the synchronous orbits at the long ends of Castalia the $\pm S$(addle) solutions, and those at the shorter ends of Castalia the $\pm C$(enter) solutions. For the given parameters of Castalia, the locations and Jacobi constant values of these orbits are:

$$\begin{aligned}
\mathbf{r}_{+S} &= (0.956,\ -.1\ 17,0.021)\ \text{km} \quad ; C_{+S} = 2.0221 \times 10^{-7}\ \text{km}^2/\text{s}^2 \\
\mathbf{r}_{-S} &= (-.910,\ -\ .041\ ,0.024)\ \text{km} \quad ; C_{-S} = 1.9535 \times 10^{-7}\ \text{km}^2/\text{s}^2 \\
\mathbf{r}_{+C} &= (0.049,0.727,0.011)\ \text{km} \quad ; C_{+C} = 1.6755 \times 10^{-7}\ \text{km}^2/\text{s}^2 \\
\mathbf{r}_{-C} &= (0.020,\ -.744,\ 0.006)\ \text{km} \quad ; C_{-C} = 1.6672 \times 10^{-7}\ \text{km}^2/\text{s}^2
\end{aligned} \tag{38}$$

For Castalia all four synchronous orbits are unstable (this means that a particle perturbed slightly from any of these orbits will depart the equilibrium point in a hyperbolic fashion). The $\pm S$ orbits are hyperbolically unstable. Thus, any particle displaced from these ljody-fixed points will depart from that point on a local hyperbola. Figure 5 shows the stable and unstable manifolds of these points. Note that each of these points has stable and unstable manifolds trapped near the asteroid as well as stable and unstable manifolds trapped away from the asteroid. Each manifold is a one dimensional object in phase space (which is a generic property of such hyperbolic unstable points).

These manifolds also provide the limiting escape trajectory for a particle as follows, Suppose the particle is started from Castalia's surface with a Jacobi constant incrementally less than C_S and along the stable manifold. Then the particle will follow the stable manifold as it approaches the S equilibrium point, taking an arbitrarily long time to arrive at this point. Once in the neighborhood of the point, the particle will come under the influence of an unstable manifold. If it comes under the influence of the trapped unstable manifold it will fall back onto the asteroid. If it comes under the influence of the unstable manifold trapped away from the asteroid, it will move away from the asteroid along this manifold and will never return to the ast eroid surface.

The $\pm$ C orbits are complex unstable. 'J'bus, any particle displaced from these orbits will depart from that point on a (locally) hyperbolic spiral. lath of these manifolds is a 2-dimensional object in phase space and cannot be traced out as the hyperbolic manifolds of the $\pm S$ orbits could be. Figure 5 also shows particular trajectories from the stable and unstable manifolds of the $\pm C$ orbits. These manifolds tend to lie in the equatorial plane of Castalia, and cause the radius of the trajectory to oscillate in an unstable manner, thus causing either close approaches to, or impact with, the asteroid.

The instability of the $\pm$ C equilibrium points highlights a classification that can be applied to Castalia (and to any uniformly rotating asteroid). The classification, as originally defined (Scheeres, 1994), applies to any body with 4 synchronous orbits. If two of these orbits are unstable (the S orbits) and two of these orbits are stable (the C orbits), then the asteroid is classified as Type I. If all four of the orbits are unstable, as with Castalia, then the asteroid is classified as Type 11. Note that the ,S orbits are always unstable.

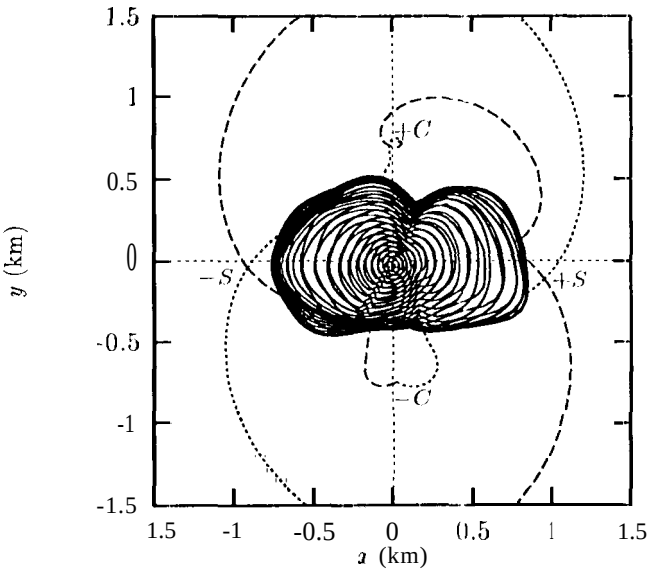

Figure 5: Segments of the Stable & Unstable Manifolds of the Equilibrium Points. Stable manifolds are dotted lines, unstable manifolds are dashed lines.

4.3 Periodic Orbit Families

We also computed families of periodic orbits about the asteroid. The computation of these orbits requires a precision integration routine and a set of software tools which allow's one to force the end-points of an orbit to coincide. The details of performing such a computation involves the use of Poincaré maps and Newton-Raphson iteration. Given one periodic orbit, other members in its family may be found via analytic continuation of the orbit with respect to some parameter, usually the Jacobi constant or the orbit period.

There are 3 main families of periodic orbits close to an asteroid such as Castalia: equatorial direct, equatorial retrograde and non-equatorial. The retrograde orbits exist as circular orbits far from the asteroid and continue for decreasing radius until they intersect the asteroid itself. The direct orbits exist as circular orbits far from the asteroid and continue for decreasing radius until they approach the radii of the synchronous orbits. Then they split into elliptic orbits (with additional complications not studied here) and can be continued until they intersect the asteroid. The non-equatorial orbits exist only in the vicinity of certain radii where the out-of-plane (nodal) period of the orbit is commensurate with the rotation rate of the asteroid. In the case of 1:1 commensurability these orbits are continued from halo orbits associated with the four equilibrium points discussed above. As the orbital period of this family is varied, the inclination varies, approaching $i = 90$. The families associated with the 1:1 commensurability are all unstable. Other families may exist at different values of commensurability.

Figures 6- 11 present members of each of these periodic orbit families in the Bodly-fixed coordinate frame. Figure 6 presents some select members of the direct, equatorial family of periodic orbits about Castalia. This family begins as a family of circular orbits when far from Castalia (solid line) and then bifurcates iuto two families of elliptic orbits when close to Castalia (dashed and dotted lines). The two bifurcated branches of the family are close to being symmetric about the y axis, and would be if Castalia were symmetric about this axis.

Figure 7 presents members of a family of retrograde, equatorial periodic orbits that also begins as a family of circular orbits far from Castalia, and remains essentially circular as it draws closer to the surface of Castalia. This family is stable up to grazing orbits, except for a small

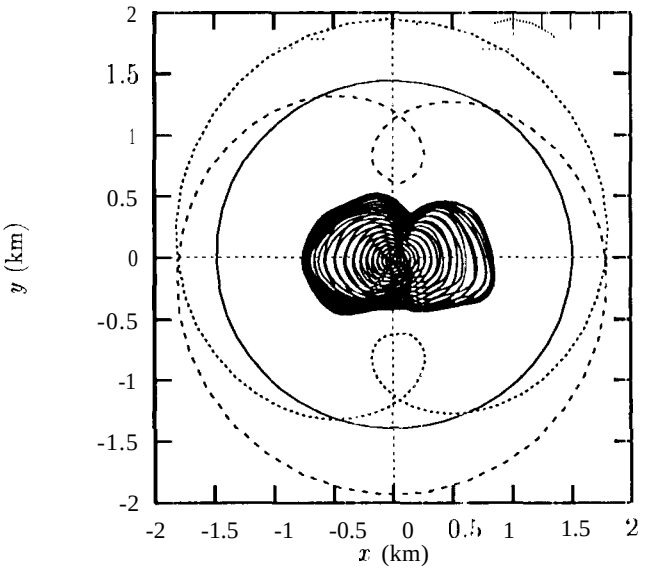

Figure 6: Direct, Equatorial Periodic 01 bits About Castalia

interval bounded by the two dashed lines in Figure 7. The existence of the stable family indicates that it is possible for particles to orbit very close to the asteroid surface for extended periods of time.

Figures 8 - 10 depict members of a periodic orbit family that is comprised of orbits with a non-zero inclination. Ideally, this family originates at the halo orbits associated with the $\pm C$ equilibrium points and terminates at the halo orbits associated with the $\mp S$ equilibrium points (or vice-versa). For Castalia this family does not complete such a path, because it intersects with the longer ends of the asteroid as it moves from the $\pm C$ point to the $\mp S$ point. The figures give projections of some select members of this family into the x-y, x-z and y-z planes. Castalia is not drawn on these figures as the orbits would be covered in some cases. All members of this family are unstable. A similar family also exists, ideally traversing from the $-C$ equilibrium point through a polar orbit to the $+S$ equilibrium point. For densities larger than 3 g/cm^3 this family will not intersect the asteroid. Due to the unstable nature of these orbits their manifolds permeate the phase space close to the asteroid surface, thus low speed ejecta from Castalia evolve under the influence of these manifolds. These manifolds will intersect with Castalia's surface or, barring that, will escape from the vicinity of the asteroid.

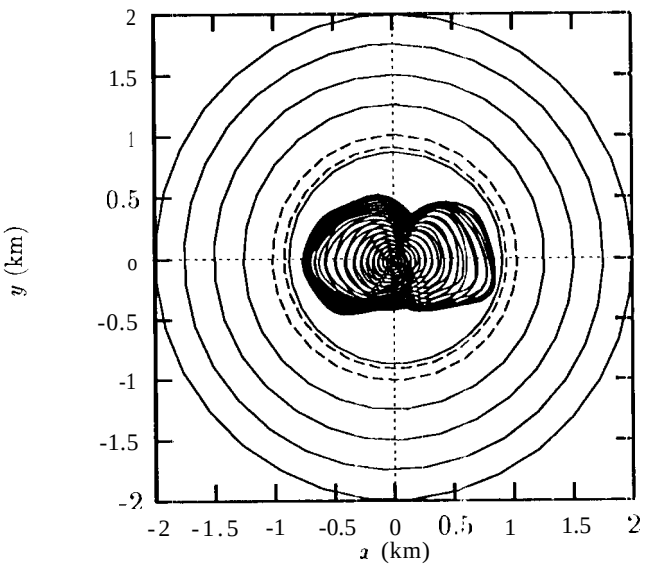

Figure 7: Retrograde, Equatorial Periodic Orbits About Castalia

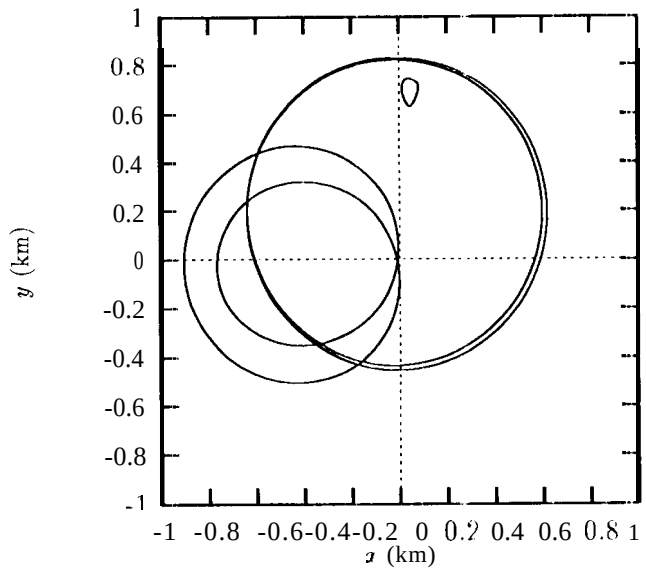

Figure 8: x-y Projection of Non-Equatorial Periodic orbits About Castalia

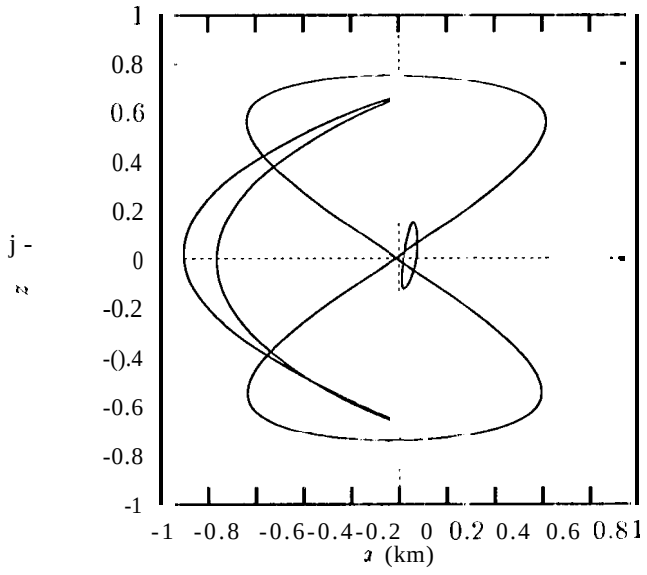

Figure 9: x-z Projection of Non-Equatorial Periodic 01 bits About Castalia

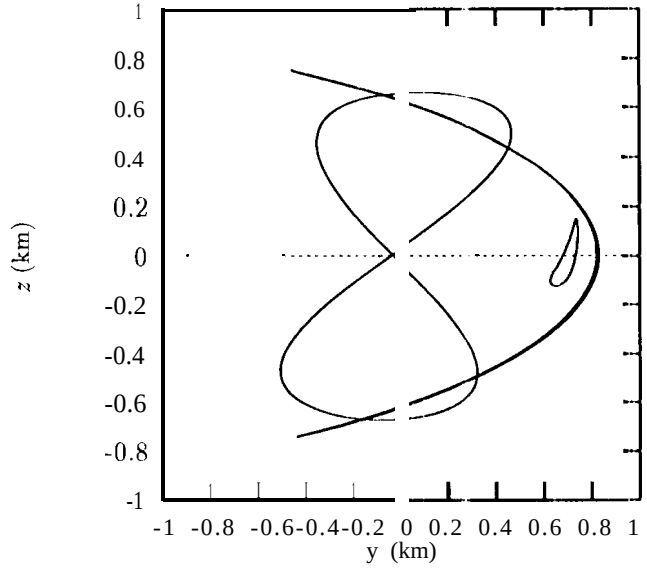

Figure 10: y-2 Projection of Non-Equatorial Periodic Orbits About Castalia

Figure 11: Three-dimensional views of non-equatorial periodic orbits

The stability of these periodic orbits affects the nature of motion in the surrounding phase space. If a family is stable, then neighboring trajectories will oscillate about it and will not diverge exponentially from it. If the family is unstable, then neighboring trajectories will diverge exponentially from it and will wander over a region of phase spare in general. If such an unstable orbit lies close to the asteroid, then the usual case is for the divergent trajectory to intersect the asteroid, or to suffer close approaches which send the trajectory away on a hyperbolic orbit. Figure 12 is a plot of the normalized Jacobi constant of a periodic orbit family member vs the periodic orbit periapsis and apoapsis. If the orbit is stable, it is represented by a solid line, if unstable, by a dotted line. The periapsis and apoapsis of each orbit is drawn, so a horizontal line drawn from a particular value of the normalized Jacobi constant will intersect the periodic orbit periapsis first, and the apoapsis second. Note that the retrograde orbits (negative Jacobi constant) are nearly circular,

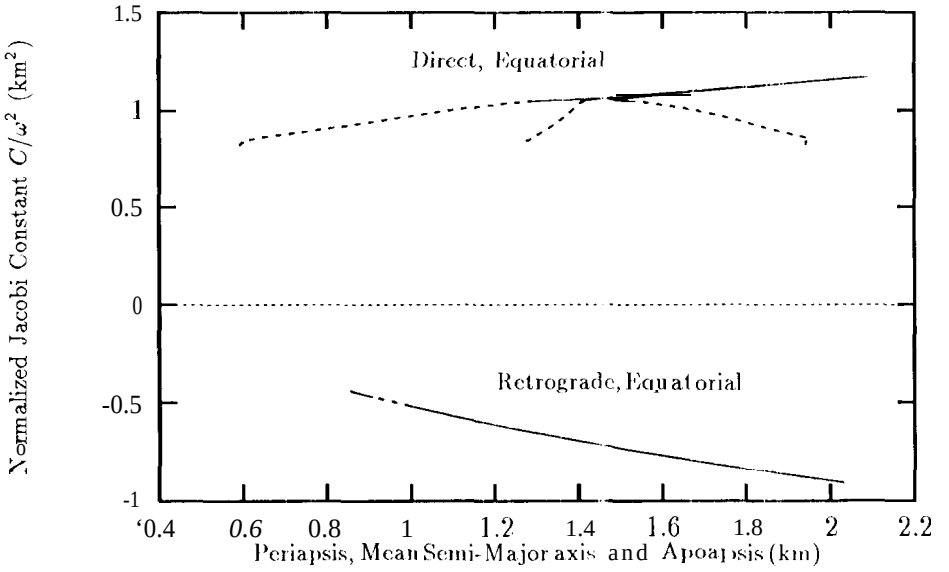

Figure 12: Periodic Orbit Family Stability. Plotted is the periapsis, mean semi-major axis and apoapsis of the direct and retrograde equatorial orbit families. The solid lines indicate stable members, the dashed lines indicate unstable members.

4.4 Ejection and Capture Dynamics

One of the most interesting aspects of dynamics shout asteroids is the possibility for a given orbit to be ejected into a hyperbolic escape trajectory, or conversely for a hyperbolic orbit to be captured into an elliptic orbit. The possibility of these occurrences was first communicated to the authors by J .1{. Miller (personal communication). Such effects provide mechanisms for an asteroid to shed ejecta, capture non-ejecta particles on its surface and temporarily capture neighbors of the asteroid.

4.4.1 Resonance Effects

The expected change in Keplerian energy and radius of periapsis and apoapsis due to particle interaction with the 2nd order gravitational harmonics can be derived as follows. Restricting ourselves to the gravity potential of 2nd order only, which provides the major perturbations to the

orbits, from Equations 23, 28 and 29 we have

$$U_2 = \frac{\mu}{r^3}\left[\frac{r_o^2 C_{20}}{2}\left(3\sin^2\alpha - 1\right) + 3r_o^2 C_{22}\left(1 - \sin^2\alpha\right)\cos(2\lambda)\right] \tag{39}$$

where $\sin\alpha = \sin i \sin u$, $u = \nu + f$ and λ is the particle longitude in the body-fixed coordinate system. This formula is specialized to the case of an equatorial elliptic orbit.

Let us estimate the total variation one may expect in the apse radii from one periapsis passage is derived. We assume that the orbital motion takes place in the equatorial plane, so $\sin\alpha = 0$, $\cos\alpha = 1$ and $\lambda = f + \nu - \omega t$, and assume that the equation is evaluated in the vicinity of periapsis. Later we shall perform a quadrature of the equation about the periapsis passage, so let us neglect any terms of the differential equations which are odd about the periapsis passage. Restricting ourselves thusly yields the following simplified formulae:

$$\dot{C}_2 \approx \frac{9\mu e r_o^2 C_{22}\dot{f}}{a(1-e^2)r^2}\sin 2\nu \sin f \sin 2(f-\omega t) - \frac{6\mu r_o^2 C_{22}\dot{f}}{r^3}\sin 2\nu \cos 2(f-\omega t) \tag{40}$$

$$\dot{r}_p \approx \frac{9r_p^2 r_o^2 C_{22}\dot{f}}{a(1-e^2)r^2}\sin 2\nu \sin f \sin 2(f-\omega t) + \frac{6r_p^2 r_o^2 C_{22}\dot{f}}{er^3}\left(1-\frac{r^2}{r_p^2}\right)\sin 2\nu \cos 2(f-\omega t) \tag{41}$$

$$\dot{r}_a \approx \frac{9r_a^2 r_o^2 C_{22}\dot{f}}{a(1-e^2)r^2}\sin 2\nu \sin f \sin 2(f-\omega t) - \frac{6r_a^2 r_o^2 C_{22}\dot{f}}{er^3}\left(1-\frac{r^2}{r_a^2}\right)\sin 2\nu \cos 2(f-\omega t) \tag{42}$$

(43)

where the true anomaly rate is $\dot{f} = \pm\sqrt{\mu a(1-e^2)}/r^2$, positive for direct motion and negative for retrograde motion.

To estimate the effect of a periapsis passage on these elements, let us introduce some assumptions which allow for a simple quadrature. First, assume that $r \approx r_p$ through the flyby, that $f \approx \dot{f}_p t$ around the flyby, and finally that the osculating elements are nominally conserved during the closest approach. This allows a quadrature about the periapsis flyby from time $-T$ to time $+T$. Note the following results:

$$\int_{-T}^{T}\cos 2\left(\omega - \dot{f}_p\right)t\,dt = \frac{\sin 2\left(\omega - \dot{f}_p\right)T}{\omega - \dot{f}_p} \tag{44}$$

$$\int_{-T}^{T}\sin \dot{f}_p t \sin 2\left(\omega - \dot{f}_p\right)t\,dt = -\frac{\sin\left(2\omega - 3\dot{f}_p\right)T}{2\omega - 3\dot{f}_p} + \frac{\sin\left(2\omega - \dot{f}_p\right)T}{2\omega - \dot{f}_p} \tag{45}$$

Performing the quadrature yields the formulae:

$$\Delta C_2 \approx -\frac{3\mu r_o^2 C_{22}\dot{f}_p}{r_p^3}\sin 2\nu \left[\frac{2\sin 2\left(\omega - \dot{f}_p\right)T}{\omega - \dot{f}_p} + \frac{3e}{1+e}\left\{\frac{\sin\left(2\omega - 3\dot{f}_p\right)T}{2\omega - 3\dot{f}_p} - \frac{\sin\left(2\omega - \dot{f}_p\right)T}{2\omega - \dot{f}_p}\right\}\right] \tag{46}$$

$$\Delta r_a \approx -\frac{9r_o^2 C_{22}\dot{f}_p}{a(1-e^2)}\left(\frac{r_a}{r_p}\right)^2 \sin 2\nu \left[\frac{1}{3}\left(1+\frac{r_p}{r_a}\right)\frac{\sin 2\left(\omega-\dot{f}_p\right)T'}{\omega-\dot{f}_p} + \frac{\sin\left(2\omega-3\dot{f}_p\right)T'}{2\omega-3\dot{f}_p} - \frac{\sin\left(2\omega-\dot{f}_p\right)T'}{2\omega-\dot{f}_p}\right] \quad (47)$$

$$\Delta r_p \approx -\frac{9r_o^2 C_{22} f_p}{a(1-e^2)} \sin 2\nu \left[\frac{\sin\left(2\omega-3\dot{f}_p\right)T'}{2\omega-3\dot{f}_p} - \frac{\sin\left(2\omega-\dot{f}_p\right)T'}{2\omega-\dot{f}_p}\right] \quad (48)$$

$$\dot{f}_p = \pm\sqrt{\frac{\mu(1+e)}{r_p^3}} \quad (49)$$

where in the current approximation $2T'$ represents the time over which the particle will receive its largest transient perturbation. A value of $T' = \pi/(4\omega)$ serves this purpose and corresponds to a time period of one-fourth of the asteroid revolution (when taken from $-T'$ to $+T'$). Note that these expressions give an estimate on the amplitude of the transient variations and not necessarily the total variation of these quantities.

'1'0 derive similar equations for an apoapsis passage, interchange all occurrences of $(-)_p$ and $(-)_a$, as well as changing the signs in front of the Δr_a and Δr_p equations. The magnitude of the effect at apoapsis is definitely smaller, aud may often be neglected unless the orbit is near circular. For a retrograde orbit the angular rates w and $\dot{f}_p$ add, so again the total magnitude of the variation is small.

4.4.2 General Results on Orbit Dynamics

The above equations provide insight into the dynamics of a particle in a direct orbit about an asteroid. The first, and most definite, result is the relation between which quadrant (Figure 13) of the asteroid contains the periapsis and changes in orbit energy. Every time a particle passes through periapsis, its argument of periapsis, denoted by ν, will lie iu one of these quadrants. Now, note that the equation for ΔC_2 is proportional to the term $-\sin 2\nu$. Thus, when the periapsis lies in quadrants 1 or III (i.e. $\nu \in [0, \pi/2], [\pi, 3\pi/2]$), $\Delta C_2 < 0$ and the energy decreases. Conversely, when the periapsis lies in quadrants 11 or IV (i.e. $\nu \in [\pi/2, \pi], [3\pi/2, 2\pi]$), $\Delta C_2 > 0$ aud the energy increases. These increases and decreases in energy cau be significantly large, and allow the asteroid to either capture a hyperbolic orbit that passes close enough to the body, or eject au elliptic orbit into a hyperbolic orbit that escapes from the asteroid. Thus a hyperbolic flyby with periapsis in quadrants I or III may be subject to capture, and au elliptic orbit with periapsis in quadrants II or IV may be subject to ejection.

For hyperbolic orbits, there is iu genera] only one pass through the system and a single chance at capture. For elliptic orbits, if not ejected from the asteroid the orbits' argument of periapsis will be randomly distributed about the asteroid from orbit to orbit. Even if some resonance originally exists in the orbit, the act of passing through periapsis will iu general destroy the resonance that existed unless the argument of periapsis lies along the divisions between quadrants) where we find closed, periodic orbits close to the asteroid. In the general case the resonances cannot be preserved, due to the timing changes from orbit to orbit. Thus, in general, an elliptic orbit will encounter many opportunities to be ejected from the system. If the flyby periapsis is in quadrants] or]]1, then the orbits' apoapsis is drawn iu towards the asteroid, which may heighten the effect of the subsequent periapsis passage. Eventually, the periapsis will lie in quadrants 11 or IV, aud ejection become a possibility. Note that a mitigating feature is that changes iu the periapsis radius move in the opposite direction of tile changes in the apoapsis radius. '1'bus, for a quadrant 1 or 111 flyby, the orbit becomes more circular and, if the periapsis radius changes by a significant amount, the subsequent orbit's periapsis may be large enough to

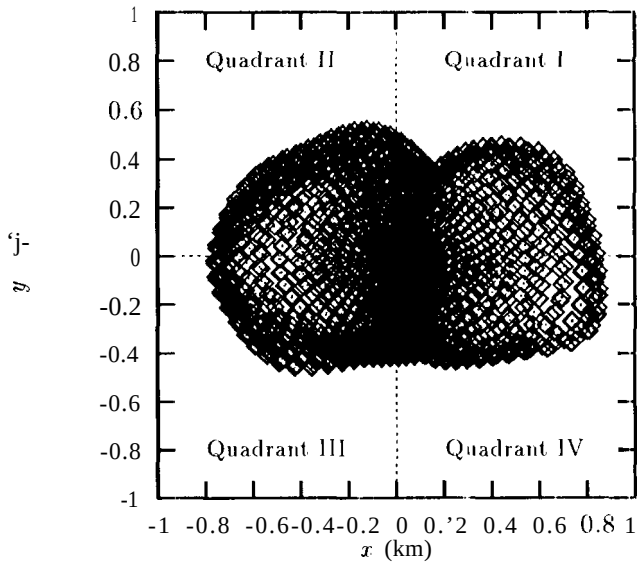

Figure 13: Quadrants 1 - IV as defined for Castalia

avoid some of the large changes. Conversely, for a quadrant II or IV flyby the orbits' periapsis will decrease in general and subject the orbit to larger perturbations on ensuing passages.

4.4.3 Capture and Escape Radius

When can one periapsis passage yield a large enough change in the Keplerian energy to either capture a hyperbolic orbit or eject an elliptic orbit ? A parabolic orbit has zero Keplerian energy, so substituting the proper terms in

$$\Delta C_2 + C_2 = 0 \tag{50}$$

yields the condition:

$$0 = 1 - e^2 + \frac{6r_o^2 C_{22} \dot{f}_p \sin 2\nu}{r_p^2} \left[\frac{2(1+e)\sin 2\left(\omega - \dot{f}_p\right)T}{\omega - \dot{f}_p} + 3e\left\{ \frac{\sin\left(2\omega - 3\dot{f}_p\right)T}{2\omega - 3\dot{f}_p} \frac{\sin\left(2\omega - \dot{f}_p\right)T}{2\omega - \dot{f}_p} \right\} \right] \tag{51}$$

where

$$\dot{f}_p = \sqrt{\frac{\mu(1+e)}{r_p^3}} \tag{52}$$

It is immediately clear that for a hyperbolic orbit to be captured its periapsis must lie in quadrants 1 or III. Conversely, for an elliptic orbit to be ejected its periapsis must lie in quadrants II or IV. The above equation defines one curve in the (r_p, e) plane for each value of ν. Orbits which lie between this curve and $e = 1$ may be subject to either capture or ejection during any periapsis passage if the passage occurs in the proper quadrant. It is important to note that an orbit lying in these regions is not guaranteed to be captured or ejected. Also, an elliptic orbit outside of the ejection region may still be ejected after several periapsis passages. Figure 14 presents this curve,

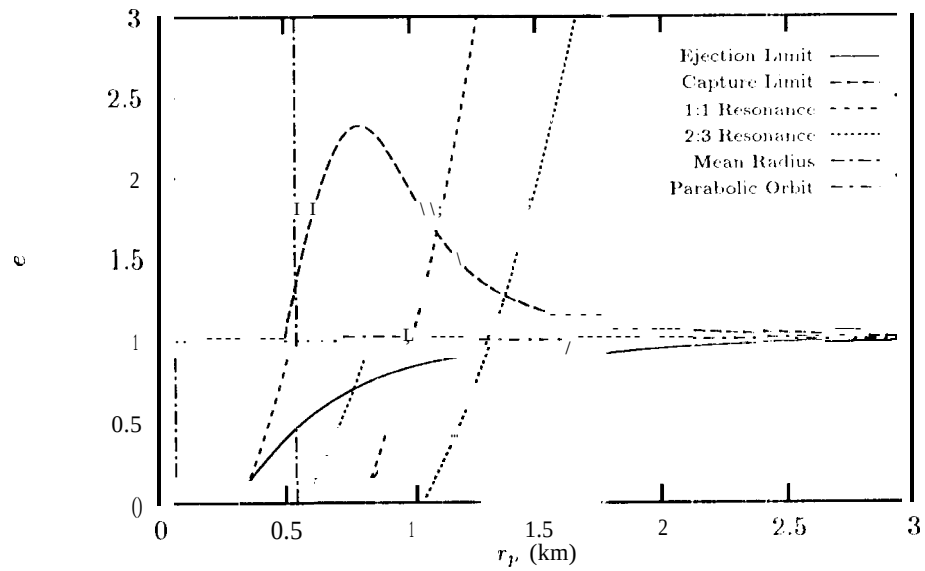

Figure 14: Limiting Conditions for Particle Capture and Ejection at Castalia

the lower curve being defined for passage through quadrants II or IV, and the upper curve for passage through quadrants 1 or III.

Figure 15 provides additional details for the capture conditions and plots the capture curve condition in terms of the periapsis radius and V_∞ of the particle. For Castalia the maximum capture V_∞ is less than $\sim$ 0.4 m/s. For larger asteroids this number may grow appreciably.

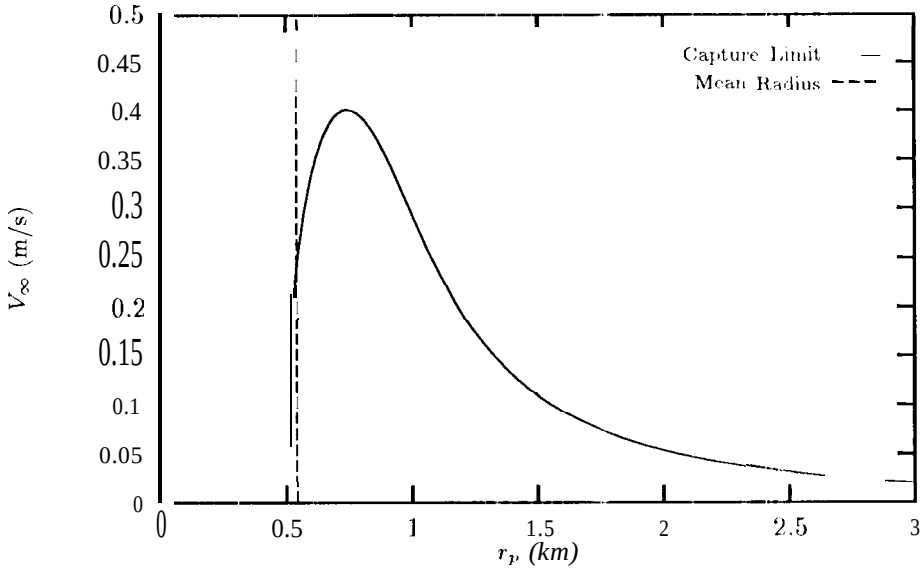

Figure 15: Limiting V_∞ for l'article Capture at Castalia

4.4.4 Resonance Effects

The 1:1 and 2:3 resonance lines in Figure 14 correspond to the periapsis radius - eccentricity combinations which provide these resonances between the asteroid rotation rate and particle true anomaly rate at periapsis. In the current formulation, the resonant term becomes proportional to e^7, so that the current results are somewhat conservative. It is expected that the change in orbital energy will be greatest when the particle lies along one of these resonance lines. Thus it is instructive to discuss them for a moment.

Consider a hyperbolic orbit which has a Castalia flyby within the capture line and along the 2:3 resonance line. Assuming that the particle is captured, its eccentricity will drop to less than one and its argument of periapsis will increase (both amounts can be estimated). Thus, after capture around the 2:3 resonance line, the orbit will move away from the resonance line, perhaps even into the region where direct ejection is not possible. In subsequent periapsis passages the apoapsis and periapsis changes are not expected to be as large, since the particle is not near the resonance line. Hence, such a capture may lead to a long-term capture of the particle in question, although the possibility for eventual escape can never be discounted.

Conversely, if a particle becomes captured at the 1:1 resonance, the subsequent orbit will lie between the two resonance lines (in the eccentricity - periapsis radius space). This particle will be much more likely to suffer an eventual ejection, as it lies near two regions where the characteristic change in orbit energy and eccentricity will be larger in general.

4.5 Retrograde Orbits

Retrograde orbits can be analyzed in terms of classical planetary orbiter results. In this situation the semi-major axis, eccentricity and inclination have only short-period variations. The argument of periapsis, argument of the ascending node and mean epoch all have a secular variation which is influenced most strongly by the gravity coefficient C_{20}. See (Scheeres, 1994) for a more in-depth discussion of this case, including higher order effects of the gravity field.

For Castalia the evolution of the mean osculating elements is approximated by:

$$a = a_o \tag{53}$$

$$i = i_o \tag{54}$$

$$e = e_o \tag{55}$$

$$\Omega = \Omega_o - 3.35 \times 10^{-5} \frac{t \cos i}{a^{7/2}(1-e^2)^2} \tag{56}$$

$$\omega = \omega_o - 3.35 \times 10^{-5} \frac{t}{a^{7/2}(1-e^2)^2} \left[\frac{5}{2}\sin^2 i - 2\right] \tag{57}$$

$$M_o = M_{o_o} + t\left(\frac{3.07 \times 10^{-4}}{a^{3/2}} - 3.35 \times 10^{-5} \frac{t}{a^{7/2}(1-e^2)^{3/2}} \left[\frac{3}{2}\sin^2 i - 1\right]\right) \tag{58}$$

where the time is measured in seconds and the semi-major axis in km. For example, a circular orbit with radius 1 km will have a secular nodal rate up to -- 1660/day, which is quite large.

Note that if the periapsis radius of the orbit becomes small and the eccentricity becomes large, that the retrograde orbits may also be subject to some of the large perturbations felt by the direct orbits. In these situations one also observes the onset of chaotic dynamics. Note that, from the retrograde family of periodic orbits, we see that near circular orbits are definitely stable up to a radius of 1 km, and are possibly long-term stable within a radius of $\sim$ 0.9 km.

5 Dynamics of Surface Particles

In this section we derive the local accelerations acting on a particle as a function of surface location on Castalia by computing the local slope at each point of its surface. Then we investigate the dynamics of ejecta launched from the sur-face of the the asteroid. It is desirable to characterize the final evolution of an ejected particle given its surface location and launch velocity, and to characterize where on the surface ejecta may accumulate. This paper addresses the first concern in detail and disc. usses the second concern in light of the results found herein (see (Dobrovolskis & Burns, 1980) and (Geissler et al., 1994) for a further discussion of the second effect). The the Jacobi integral is used to derive a discriminant quantity which identifies whether or not a particle orbit may have come from the surface of the asteroid in the past, or if it may impact on the surface of the asteroid in the future. Next, some brief comments on the possible modes in which a particle may become trapped into stable orbits about the asteriod are made. Finally we discuss the dynamics and distribution of re-impact ejecta is given.

5.1 Surface Forces

The force acting on a particle at each location on the surface of the asteroid arises from gravitational and centripetal accelerations. The angle between the normal vector and the force vector at a given surface location may be related to the local slope ϕ on the asteroid surface:

$$\cos(\pi/2 - \phi) = \frac{\mathbf{n} \cdot V_{\mathbf{r}}}{|V_{\mathbf{r}}|} \tag{59}$$

For an infinitely rough surface, if the slope is less than 90° then, in general, the particle will remain fixed. If a coefficient of bulk friction is assumed for the surface, it is possible to compute the smallest angle for which a particle will be subject to sliding on the surface. Given a coefficient of friction for the surface-particle pair (μ_F), the limiting slope angle is computed as (Greenwood, 1988):

$$\mu_F = \tan\phi \tag{60}$$

Thus, for an infinitely rough surface ($\mu_F = \infty$), the limiting slope is 90°, while for a perfectly *smooth* surface (μ_F = O), the limiting slope is O°. Whereas this bulk characterization of friction is extremely simplified and does not account, for the actual physics of sliding or rolling friction, it dots provide a simple way to assign a bulk number to the surface in question. For the assumed density of 2.1 g/cm^3 the maximum slope over the surface of Castalia is 57(' which occurs at latitude of -64 and longitude of -91 degrees, near the crevice between Castalia's lobes. Figure 16 shows the contours of the slope over the surface of Castalia for a density of 2.1g/cm^3.

A friction coefficient of at least $\sim$ 1.6 would be required for a non-sliding condition to hold over the entire surface of Castalia, given the above maximum angle of 57 degrees. Previous studies have assumed a maximum slope of 33° before slipping occurs (Thomas et al., 1994), corresponding to a friction coefficient of 0.65. Thus, for the current Castalia model, there are implied slopes large enough to allow for the migration of regolith. An interesting question is what the *minimum* density of Castalia would be before all surface slopes are less than 33°. Our computation, taken over the entire surface, indicates a necessary density much larger than feasible or expected (by an order of magnitude), indicating that Castalia definitely has slopes greater than 33°.

Another quantity of interest is the minimun n density which Castalia may have before particles at the end of asteroid are thrown off by cent ripetal acceleration. This density may be computed at each point of the surface by finding the necessary density for the local normal and the local force vectors to be orthogonal. For the Castalia shape and rotation model this minin num density is 1.3 g/cm^3 and occurs at the longest end of the asteroid, as expected. This places a lower bound on the density of an unconsolidated asteroid (Burns, 1975),

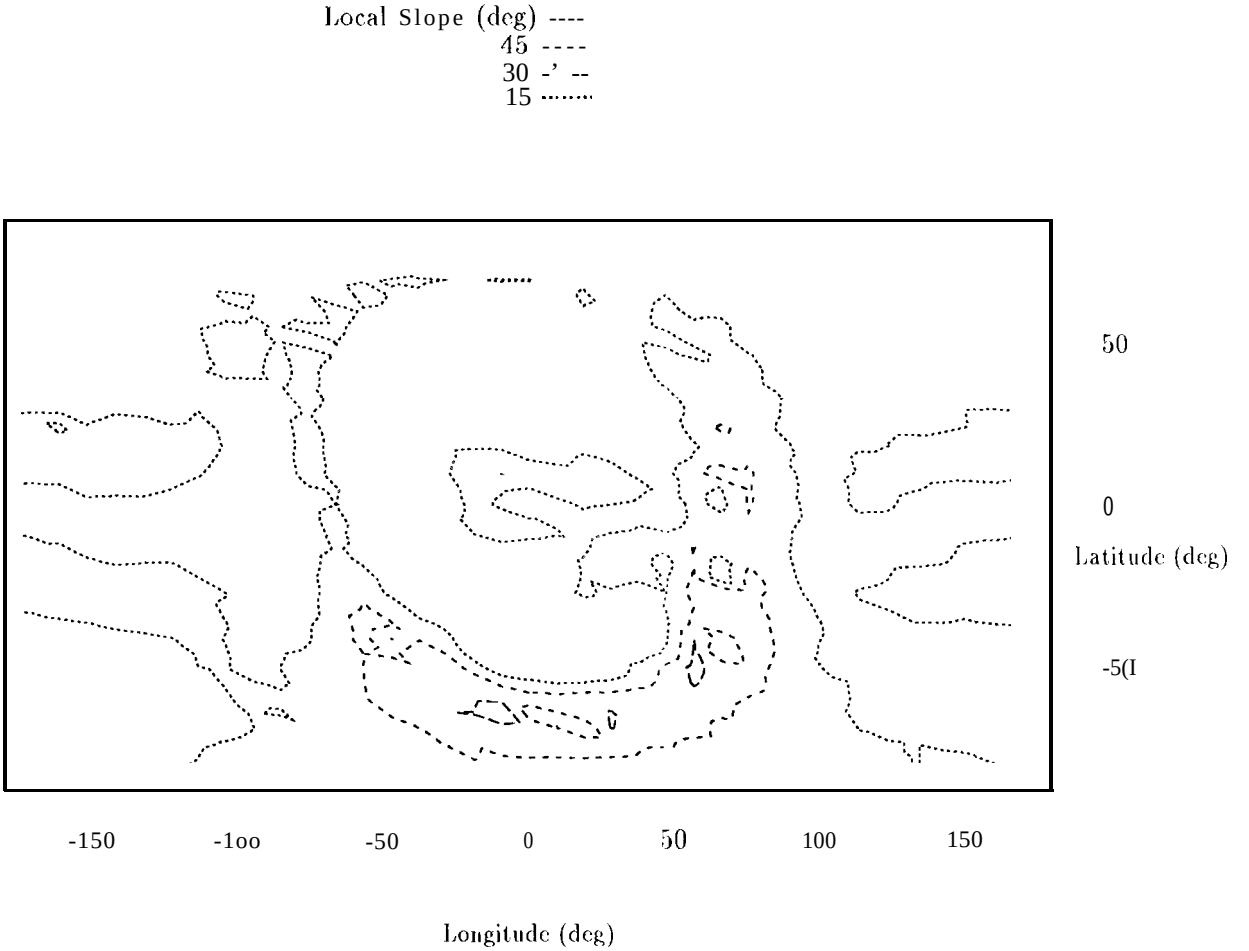

Figure 16: Slopes over the Surface of Castalia

5.2 Guaranteed Return Speed

It is possible, by using the existence of the zero-velocity curves, to derive an upper value on ejecta velocity which ensures that all ejecta velocities less than this value will eventually fall back onto the surface. This upper bound is conservative. Consider the zero-velocity curves and the $\pm S$ equilibrium points discussed previously. For values of C greater than $C_{\pm S}$ the zero-velocity curves divide the space around the asteroid into at least two distinct regions, one connected to infinity and the other(s) containing the asteroid. For the Castalia shape with a density of 2.1 g/cc, the zero-velocity curves stilt intersect the Castalia shape when $C \approx C_{\pm S}$, thus there are two disjoint components of this zero-velocity surface which contain the two ends of the asteroid. Any ejecta launched from the surface of Castalia with a Jacobi constant $C > C_{\pm S}$ will stay trapped close to the surface and will eventually reimpact the asteroid. Using this condition we can derive, as a function of position on the Castalia surface, the maximum ejecta speed which will guarantee that the ejecta will fall back onto the asteroid. For speeds greater than this speed it becomes necessary to investigate the individual trajectories to see whether or not they fall back to the surface. This speed is derived by solving the equation $J(\mathbf{r}, \dot{\mathbf{r}}) = -C_{\pm S}$ for the asteroid relative ejecta velocity $v = |\dot{\mathbf{r}}|$:

$$v = \sqrt{2(V(\mathbf{r}) - C_{\pm S})} \tag{61}$$

This result is one of several definite conclusions one may draw concerning the final evolution of ejecta. Figure 17 presents a contour plot of of the local guaranteed return speed. The limiting speeds are larger at the asteroid ends and in the crevice. The conservative nature of this bound is indicated by the regions of zero speed over the poles of the asteroid. If the assumed Castalia density were larger, these regions would also have positive guaranteed return speed.

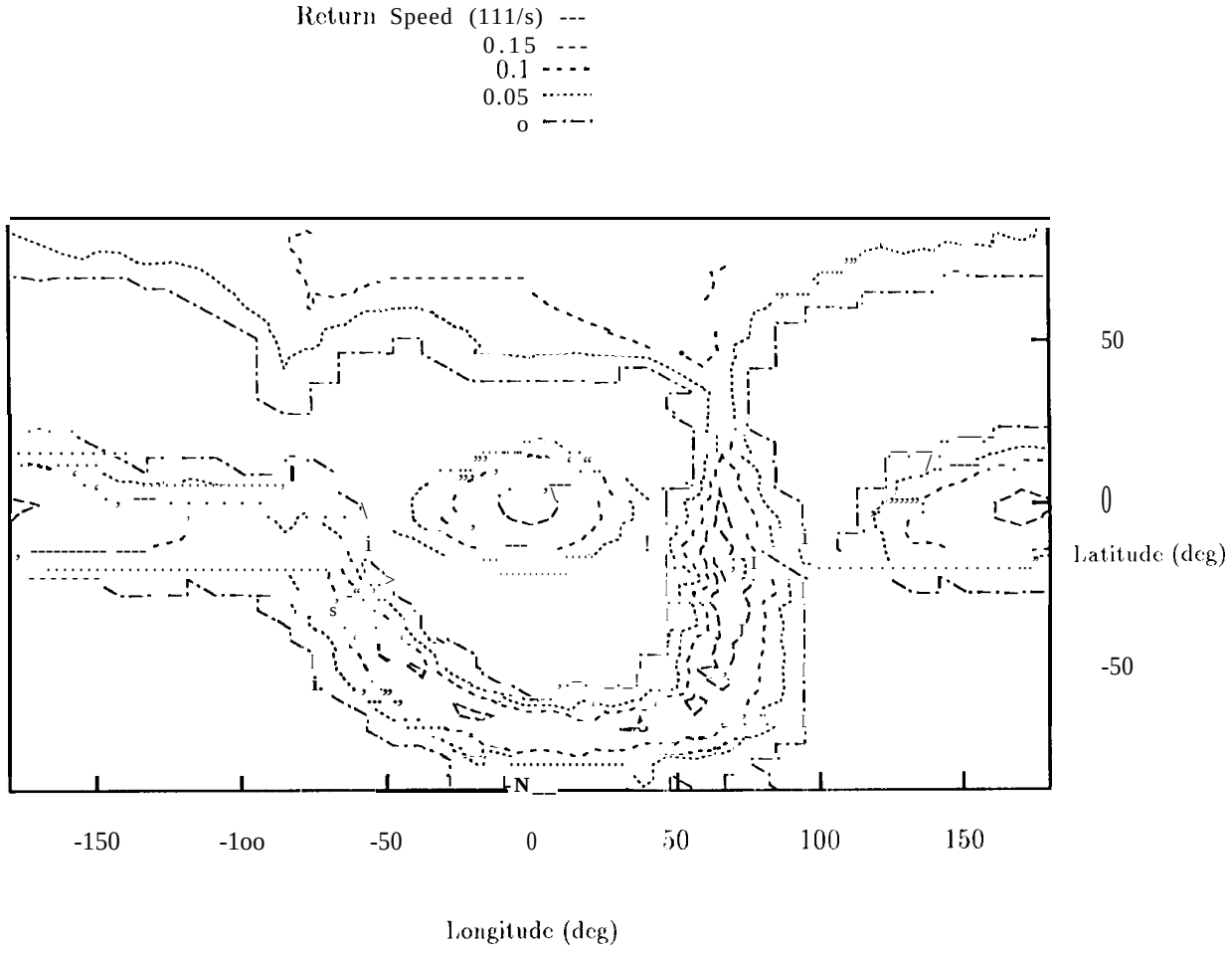

Figure 17: Guaranteed Return Speeds Over Castalia's Surface. If launch speed is less than given speed the particle returns to the surface.

5.3 Local (Normal) Escape Speed

One way to characterize how escape speeds will vary across the surface of Castalia is to evaluate the required speed normal to the local surface that is necessary to ensure escape. This dots not guarantee that the ejecta will escape (although it will be close to the true escape speed in general), but it does provide a characterization for how the actual escape speeds will vary across the surface of Castalia.

Assume that a particle leaves the asteroid normal to the local surface, or $\mathbf{v} = v\mathbf{n}$ where $\mathbf{n}$ is the local normal to the surface and v is the ejecta speed. The inertial velocity of such a particle is:

$$\mathbf{v}_I = v\mathbf{n} + \Omega \times \mathbf{r} \tag{62}$$

where $\mathbf{r}$ is the vector to the surface and Ω is the asteroid's angular velocity vector. '1'0 find the local escape speed, set the magnitude of the inertial velocity equal to $\sqrt{2U(\mathbf{r})}$. Evaluating this condition and solving the resultant quadratic equation yields:

$$v \quad \mathrm{z} \quad -\mathbf{n}\cdot(\Omega \times \mathrm{l}') + \sqrt{[\mathbf{n}\cdot(\Omega\times\mathbf{r})]^2 + 2U(\mathbf{r}) - (\Omega\times\mathbf{r})^2} \tag{63}$$

This quantity has been computed over the surface of Castalia using the polyhedral gravitational field (Figure 18) and is between 0.55 and 0.65 m/s over most of the surface. In the crevice the speeds arc over 0.65 m/s, w'hilt at the ends of the asteroid the speeds decrease to between 0.35 and 0.55 m/s.

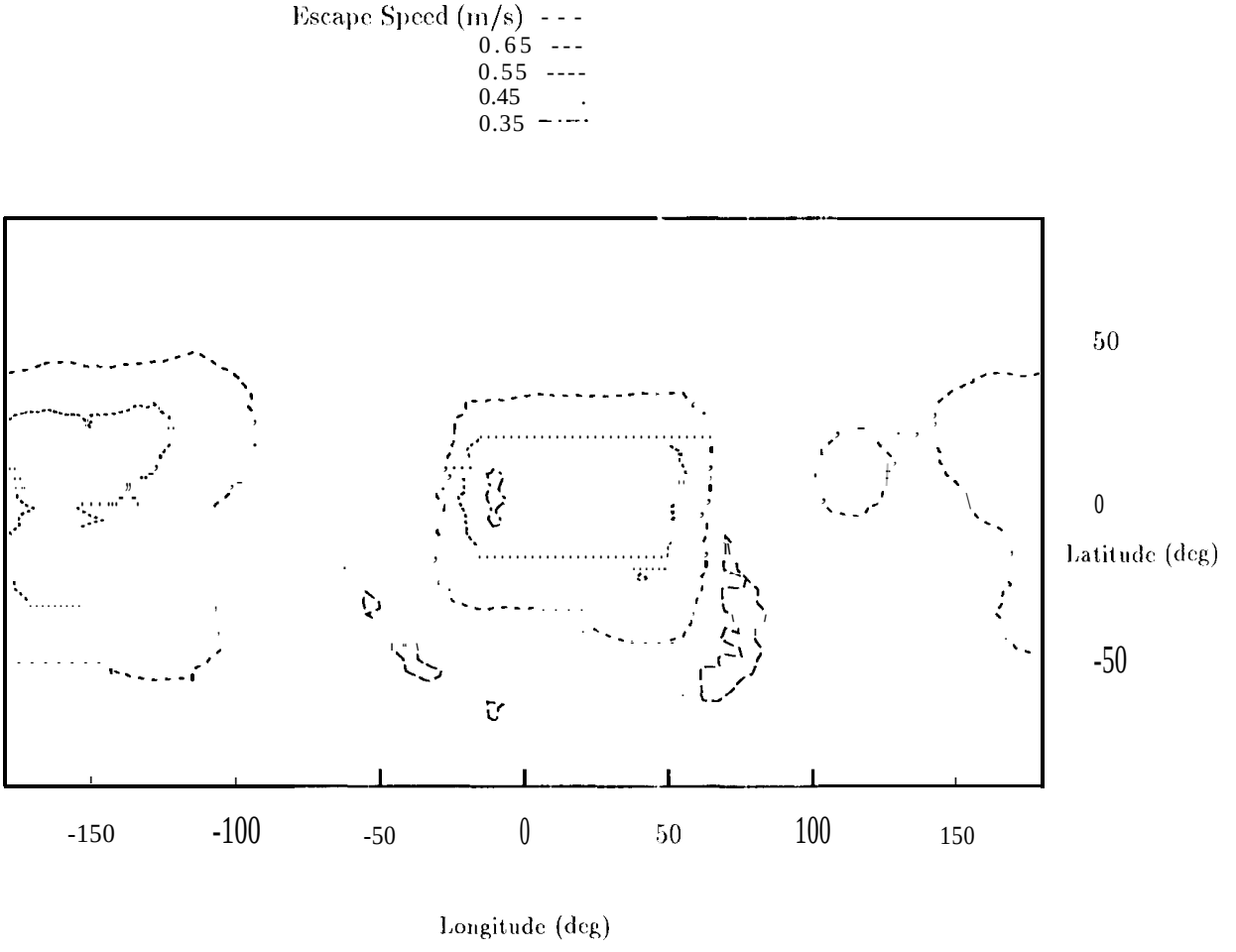

Figure 18: local Normal Escape Speed Over Cast alia's Surface. If launch speed is greater than given speed the particle will escape.

5.4 Constraints on the Origin of an Orbiting Particle

A criterion may be developed whit.11 can discriminate whether or not a particle's trajectory could either have emanated from the asteroid surface or will intersect the asteroid surface in the future. This criteria relys on the Jacobi integral and is applicable to direct, low inclination orbits.

To establish the criterion, the Jacobi integral must first be expressed in t erms of osculating orbital elements. Assume that this evaluation occurs when the particle orbit crosses the equatorial plane of the asteroid, as defined by the plane normal to the rotation pole. Then, expressing the particle orbit in terms of osculating elements and assuming that the gravitational force potential is approximated by μ/r, we find:

$$C \approx \frac{\mu}{2a} + \omega\sqrt{\frac{\mu}{a}}r(2a - r)\cos i \tag{64}$$

Next consider the Jacobi integral itself, $C = V - T_E$. Evaluating the Jacobi constant over the entire asteroid surface (assuming $T_E = 0$) yields a maximum value C^* of the Jacobi constant C. For Castalia $C^* = 2.1223 \times 10^7$ km^2/s^2 and occurs at a latitude of -17 degrees and longitude of 67 degrees. If a particle trajectory intersects the asteroid surface, that trajectory must have a Jacobi constant less than C', as can be easily inferred from the relation $C = V - T_E$ and $T_E \geq 0$. Thus if a particle orbit has a Jacobi constant C greater than C* , it does not intersect with the asteroid surface in either the future or the past.

Using the relation Equation 64, we can explicitly relate a given orbit about the asteroid with the criteria for whether it emanated from the asteroid surface. If tile inequality

$$\frac{\mu}{2a} + \omega\sqrt{\frac{\mu}{a}}r(2a - r)\ \text{Cos}\ r' > C^* \tag{65}$$

holds, then the particle's trajectory could not have originated from the asteroid surface. Note that $C' > \mu/(2a)$ in general, as $C^* > \mu/r^* > \mu/(2a)$ in general, where r^* is the radius at which the function V is maximized and a is the semi-major axis of the particle orbit in question. Thus whenever the inclination exceeds 90° the inequality is trivially false and the criterion no longer applies. In fact, as the particle inclination progressively grows from 0° to 90°, the applicability of this criterion decreases. Thus, in practice, this criterion is only useful for nearly equatorial, direct orbits. Note that Dactyl is in such an orbit about Ida (Belton et al., 1994). Allowing for tile small angle approximation, it would be valid to set $\cos i \approx 1$ for r' < 10°.

Now define two characteristic lengths,

$$\alpha = \frac{1}{2\mu}\left(\frac{C^*}{\omega \cos i}\right)^2 \tag{66}$$

$$\beta = \frac{\mu}{C^*} \tag{67}$$

where both of these values have units of kilometers. For Castalia, these constants are found to be:

$$\alpha = 1.303 / \cos^2 i \ \text{km} \tag{68}$$

$$\beta = 0.443 \ \text{km} \tag{69}$$

Finally, assume that the particle orbit is evaluated at periapsis, or $r = a(1 - e)$. In this case the inequality can be expressed in several different ways, the two of immediate interest are:

$$(1 - e^2)a^3 - 2\alpha a^2 + 2\alpha\beta a - \frac{1}{2}\alpha\beta^2 > 0 \tag{70}$$

$$(r_a - \alpha)r_p^2 + \left(r_a^2 - 2\alpha r_a + 2\alpha\beta\right) r_p - \alpha(r_a - \beta)^2 > 0 \tag{71}$$

A few quick notes on these inequalities: Condition 70 is a cubic and is useful for evaluating the condition when $e = 0$, Condition 71 is also valid if r_a and r_p arc interchanged, and can be readily

factored using the quadratic equation:

$$r_p > \frac{r_a^2 - 2\alpha r_a + 2\alpha\beta}{2(r_a - \alpha)} \left[\sqrt{1 + \frac{4\alpha(r_a - \beta)^2(r_a - \alpha)}{(r_a^2 - 2\alpha r_a + 2\alpha\beta)^2}} - 1 \right] \tag{72}$$

This inequality is plotted in Figure 19 for $i = 0$ from $r_a = r_p$ to $r_a \to \infty$. Taking the limit $r_a \to \infty$ yields the limiting inequality $r_p > \alpha$. in the figure, any particle whose orbit which falls to the right of the solid line could not have come from the asteroid surface and any particle whose orbit falls to the left of the solid line may have come from the asteroid surface.

An important point to note in the plot is that all circular orbits outside of ~ 2 km could not have originated from Castalia's surface. Recall that orbits with a mean semi-major axis within 1.4 km of Castalia's surface are unstable. Thus, this leaves only a relatively small range of direct orbits which are stable and which potentially come from the surface of the asteroid.

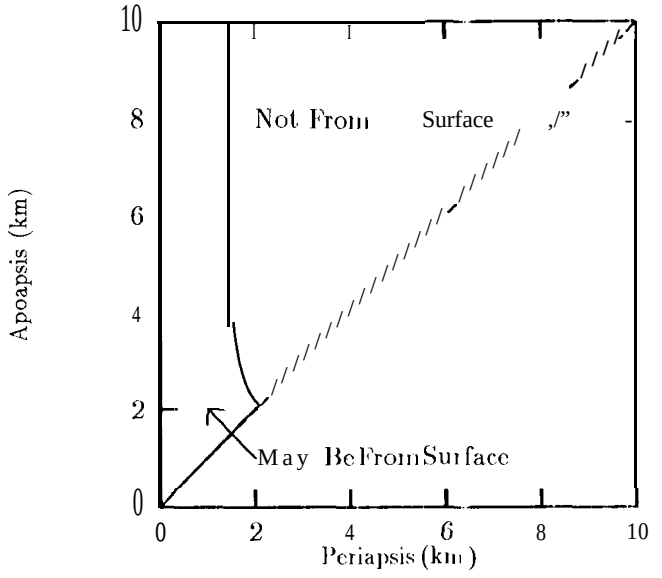

Figure 19: Ejecta Exclusion Criterion for $i = 0$

5.5 Ejects Transport into Orbit

Consider the possibility for ejecta to depart the surface of the asteroid and end in a direct trajectory which is "(stable" for some length of time. The direct family of periodic orbits provides a useful measure of how close to the asteroid surface stable orbits exist. For Castalia, members of this orbit family with periapsis inside of ~ 1.3 km are unstable (mean semi-major axis within $\sim$ 1.4 km). This places some limitations on the region where an ejecta could become trapped in a stable orbit, depicted in Figure 20.

The necessary condition for ejecta to be placed into this stable region is that the periapsis radius be raised by at least ~ 1 km. The mechanism for this to occur is during an apoapsis passage of the orbit through quadrants 1 or 111 of the asteroid. The amount of "kick" in the periapsis radius due to one apoapsis passage may range up to the order of 0.5 kilometers assuming $r_a = 1$ km and $r_p = 0.5$ km. However, after such a large change in periapsis subsequent changes will be smaller due to the higher periapsis and lower eccentricity. '1'bus, even after such a large change in periapsis a number of succesive changes would still be required to raise the periapsis into the stable region. Note that these same orbits will be subject to changes in apoapsis radius on the order of

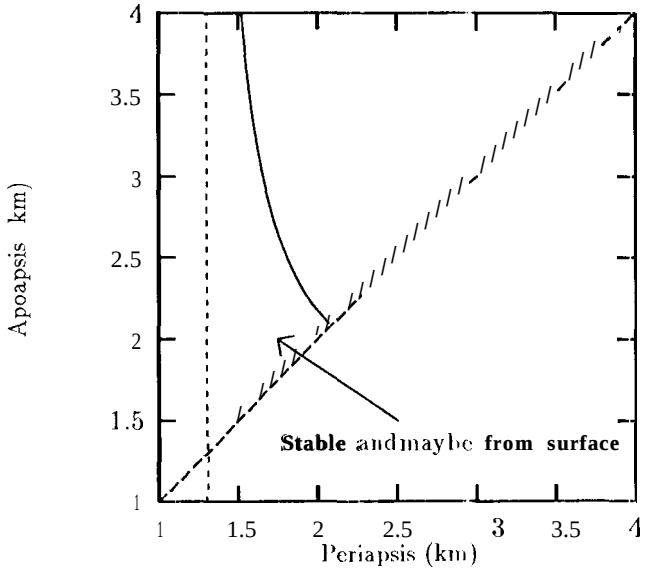

Figure 20: Stable region of direct orbits that may originate from the surface

kilometers during each periapsis passage, thus implying that it is much more likely that an ejection of the particle from the Castalia system would occur.

For retrograde orbits the situation is different. Note that the family of retrograde orbits extends all the way down to the asteroid surface, with stable orbits existing within hundreds of meters from the asteroid surface. In this situation the ejecta orbits are not susceptible to large changes in peri- and apoapsis radius, and thus a mechanism like that for direct orbits may not apply.

A more likely scenario follows. Consider that an impact between asteroids may effectively disperse a portion of the asteroid into some velocity distribution. All that is required is that some members of the velocity distribution be given speed of $\sim$ 0.7 km/s in a retrograde direction, and that the initial radius of the particle, as measured from the asteroid center of mass, is large enough for the particle's trajectory to avoid the longer ends of the resulting asteroid. Thus this scenario implicitly implies that one of the longer cuds of the asteroid is removed in the collision.

5.6 Distribution of Re-Impact Ejects

An important issue to address is the expected distribution of re-impact ejecta over the surface of Castalia. There are two approaches one may take to derive estimates of these distributions. The first, and simplest, is to identify regions of the Castalia surface which have large slopes (as defined earlier). Return ejects in these regions will be susceptible to migration. The second is to characterize the trajectories of ejecta and map these back to the surface again.

5.6.1 Surface distribution

Note from Figure 16 that the regions of lowest slope range over the north pole and cover the regions of each lobe half-way between the long ends and the crevice. The southern pole has a uniformly higher slope. In the vicinity of the long ends of the asteroid (around longitude 0° and 1800), the slopes tend to be higher, although they do not exceed 1.5° , so one may not expect much migration away from the ends of the asteroid. Indeed, the cuds of Castalia seem to be blunted, perhaps indicating that natural processes have already shaped the ends of the asteroid.

The Castalia crevice exhibits the largest slopes, as would be expected. In the interior of the crevice these slopes exceed 45°, large enough for one to expect the free migration of any loose regolith. In these regions, however, one would expect the regolith to flow into the crevice and, over time, fill it up. Thus, whatever the current slope structure of the crevice, it would grow steeper as one moves back in time to the original event when the current Castalia was formed. For the current Castalia the flow of regolith would go from the southern pole, from the longitude area around $\sim$ 70° and potentially from the latitudes just south of the 180° longitude into the crevice which extends from the south of the 0° longitude in a semi-circle (in latitude-longitude space) to the equator at $\sim$ 70°.

For the current Castalia, a uniform influx of ejecta would produce a fairly uniform blanketing over the north pole, ends and over most longitudes at the equator. over the southern hemisphere one would expect a more dynamic situation with regolith flow into the crevice. In order to infer an historical interpretation of past regolith redistribution, we would be fore.cxl to consider the geometrical shape of each lobe and apparent contact points, among other issues. Note that while the southern hemisphere has the largest slopes, indicating a preferred direction for regolith flow, the two lobes are widely seperated there. Thus, influx of regolith, even over long time spans, may not be adequate to "fill-in" this crevice.

5.6.2 Dynamics of ejecta

The distribution of re-impact ejecta is a very complex problem for several reasons. First, the parameter space over which one must search to generate global results (latitude, longitude and initial velocity vector) is very large. Second, given the severe distortion in Castalia's gravity field analytical methods for mapping the ejecta dynamics close to the surface will not give an accurate or true picture. The "brute force" approach to investigating this question would be to perform a Monte Carlo analysis where the parameter space is sampled with some bounds on the velocity sampling. Some work has been done with this approach by other authors (Geissler et al., 1994) using a simple shape model (a tri-axial ellipsoid) and a restricted velocity space (constrained to be normal to surface). We plan to perform a similar analysis with the current model in the future, probably using a parallel computer. In the work of Geissler, they noted the tendency of the re-impact ejecta to accumulate on the "leading-edges') of the asteroid Ida. Moreover, the ejecta which tended to accumulate in these regions had initial speeds near escape speed.

For the Castalia model the leading edges would be longitudes in the approximate ranges $0° \rightarrow 45°$ and $180° \rightarrow 225°$. That a uniformly falling field of ejecta would tend to re-impact along the leading edges of the asteroid can be seen using a simple analysis under the assumption that the ejecta leave the surface near escape speed. As viewed from inertial space the ejecta orbits will then tend to have larger eccentricities and hence apoapsis radii far from the asteroid. Thus, after leaving the asteroid surface, they will travel far enough from the asteroid so that their orbits will be qualitatively similar to standard Keplerian ellipses. On their initial return to the asteroid, then, they may be crudely modeled as infalling particles on nearly straight lines, fixed in inertial space. Given such a situation, it is obvious that the leading edges of the rotating asteroid will, as a consequence of their travel, move into these infalling orbits as time progresses. The trailing edges of the asteroid will, instead, move away from these infalling, orbits, Thus, one would expect to see a bias toward re-impacts on the leading edges of an asteroid, at least when considering ejecta leaving close to escape speeds.

When the ejecta speeds are lower the dynamics become much more complicated and such a simple analysis dots not apply. Castalia escape speeds are very small (Figure 18), much less than the expected impact velocity of an interloper (which causes the initial ejecta field). Thus only a small fraction of ejecta will potentially fall back onto the asteroid. The fraction of ejecta whose speeds are less than escape speed will follow an essestially chaotic orbit about the asteroid until they either escape or return. (DeJong & Suzuki, 1995) depicts a number of specific trajectories

shout the asteroid Castalia, including a re-impacting ejects trajectory and an escaping ejecta trajectory. Both of these trajectories are very complex, and both will change substantially given slightly different, starting conditions. Their complex nature highlights the difficulties in arriving at general results concerning ejecta re-distribution for low speed ejecta. For ejecta speeds which are very small the ejecta distribution will begin to mimic distribution patterns that are normally encountered 011 more massive bodies, with the ejecta being distributed in the vicinity of the impact site.

6 Conclusions

In this paper we gave a general analysis of the dynamics of close orbits to the asteroid 4769 Castalia. All the results were possible due to the existence of the radar derived shape and rotation model. The majority of the computations carried out in this paper can be generated automatically once the model of an arbitrary uniformly rotating asteroid is given. Thus this paper outlines a potential analysis program for classifying asteroids in terms of the expected dynamics close to the body.

'1'here are several areas touched on in this paper where additional analysis is still needed. The predictions of the asteroid capture and ejection radius need further investigation. Issues here include the probability of capture and the likely lifetime of a captured particle. Also, the potential role of the resonances needs to be addressed, as they may significantly influence this phenomenon.

The distribution of impact ejecta over the surface of au asteroid is an area of research whose surface has been barely scratched. Future research can focus in two main areas. The first would expand upon the analytical approaches derived in this paper to estimate the final evolution of ejecta. The other would approach the problem as a numerical experiment. This would retail Monte Carlo simulations taken over the entire asteroid surface and simulations of the evolution of specific impact velocity fields.

A Gravity Coefficients

Following are the Castalia gravity coefficients through order 4. These coefficients are normalized, as defined in (Kaula, 1966), computed with respect to a normalizing radius $r_o = .5431$ km. The general form of the gravitational field can be expressed as:

$$U = \sum_{l=0}^{\infty} \sum_{m=0}^{\infty} \left(\frac{r_o}{r}\right)^{l+1} P_{lm}(\sin\phi)\left[C_{lm}\cos m\lambda + S_{lm}\sin m\lambda\right] \tag{73}$$

where P_{lm} are the normalized Legendre polynomial, ϕ is the spacecraft latitude and λ is the spacecraft longitude in the body-fixed frame.

Order	Degree	C Coefficient	S Coefficient
0	0	1.0	
1	0	0.0	
1	1	0.0	0.0
2	0	-.110298	
2	1	0.0	0.0
2	2	.156733	0.0
3	0	-.015112	
3	1	-.037935	.001211
3	2	.006325	.000616
3	3	.020568	-.013715
4	0	.036630	
4	1	.002706	.000407
4	2	-.051363	.003949
4	3	.006140	-.001747
4	4	.050334	-.006839

Table 1: Castalia Gravity Field Coefficients through Order 4

Acknowledgments

Part of this research was carried out by the Jet Propulsion laboratory, California Institute of Technology, under contract with the National Aeronautics and S'pace Administration.

References

Belton, M .J .S. et al., 1994. Determination of the orbit of (243) Ida and the mass of 243 Ida, Bull. Amer. Astron. Soc., 25.01, (abstract).

Burns, J. A., 1975. The angular momentum of solar system bodies, *Icarus*, **25**, 545-554.

Chauvineau, B., 1'. Farinella & F. Mignard, 1993. Planar orbits about a Triaxial Body: Application to Asteroidal Satellites, *Icarus*, **105**, 370-381.

Cintala, M.J., J .W. Head, L. Wilson, 1979. The Nature and Effects of Impact Cratering On Small Bodies. In *Asteroids ('I'.* Gehrels ccl.), pp 579 - 600, University of Arizona Press.

DeJong, E., S. Suzuki, 1995. Video.

Dobrovolskis, A.R., J .A. Burns, 1980. Life near the Roche Limit: Behavior of Ejecta from Satellites Close to Planets, *Icarus*, 42, 422-441.

Geissler, P.E. et al., 1994. Erosion and regolith redistribution on 243 Ida and its Moon, Bull. Amer. Astron. Sot.., 25.12, (abstract).

Greenwood, D.T., 1988. *Principles* oj *Dynamics, 2nd Ed.*, Prentice-Hall.

Hamilton, D.P., J.A. Burns, 1991. Orbital Stability Zones about Asteroids, *Icarus*, 92, 118 - 131.

Harris, A. W., 1987. On the evolution of meteroid collision debris in orbit about asteroids, Bull. Amer. Astron. Sot., 19:909, (abstract,).

Hudson, R. S., S.J. Ostro, 1994. Shape of Asteroid 4769 Castalia (1989 PB) from Inversion of Radar Images. *Science*, 263, 940- 943.

Kaula, W.M., 1966. *Theory* oj *Satellite Geodesy*, Blaisdell.

MacMillan, W.D., 1930. *The Theory* oj *the Potential*, McG raw-hill.

McKay, D.S., T.D. Swindle, R. Greenberg, 1989. Asteroidal Regoliths: What we do not know *Asteroids II* (R.]'. Binzel, '1'. Gehrels & M.S. Matthews, Eds.), pp 617- 642, 11. of Arizona Press.

Miller, J.K., 1993, *private communication.*

Petit, J. M., R. Greenberg, 1'. Geissler, 1994. Orbits around a small, highly elongated asteroid, Bull. Amer. Astron. Sot.., 25.13, (abstract).

Scheeres, 1). J., 1995. Analysis of Orbital Motion Around 433 Eros, *J. Astronautical Sciences*, 43, 4, *in* press

Scheeres, D. J., 1994. Dynamics About Uniformly Rotating, Tri-axial Ellipsoids, *Icarus*, 110, 2, pp 225 - 238

Thomas, P.C., et al., 1994. The shape of Gaspra, *Icarus*, **107**, (l), pp 23 - 36.

Weidenshilling, S. J., P. Paolicchi, V. Zappala, 1989. Do Asteroids Have Satellites? In *Asteroids II* (R.]'. Binzel, '1'. Gehrels & M.S. Matthews, Eds.), pp 643- 658, University of Arizona Press.

Werner, R. A., 1994. The Gravitational Potential of a Homogeneous Polyhedron, *Celestial Mechanics*, **59**, *253-278.*